5

Silicon Solar Cells: Structural Properties of Ag-Contacts/Si-Substrate

Ching-Hsi Lin, Shih-Peng Hsu and Wei-Chih Hsu
Industrial Technology Research Institute ,
Taiwan, R.O.C.

1. Introduction

The screen-printed silver (Ag) thick-film is the most widely used front side contact in industrial crystalline silicon solar cells. The front contacts have the roles of efficiently contacting with the silicon (Si) and transporting the photogenerated current without adversely affecting the cell properties and without damaging the p-n junction. Although it is rapid, has low cost and is simplicity, high quality screen-printed silver contact is not easy to make due to the complicated composition in the silver paste. Commercially available silver pastes generally consist of silver powders, lead-glass frit powders and an organic vehicle system. The organic constituents of the silver paste are burned out at temperatures below 500°C. Ag particles, which are ~70-85wt% and can be different in shape and size distribution, show good conductivity and minor corrosive characteristics. The concentration of glass frit is usually less than 5wt %; however, the glass frit in the silver paste plays a critical role for achieving good quality contacts to high-doping emitters. The optimization of the glass frit constitution can help achieve adequate photovoltaic properties.

The melting characteristics of the glass frit and also of the dissolved silver have significant influence on contact resistance and fill factors (FFs). Glass frit advances sintering of the silver particles, wets and merges the antireflection coating. Moreover, glass frit forms a glass layer between Si and Ag-bulk, and can further react with Si-bulk and forms pin-holes on the Si surface upon high temperature firing.

This chapter first describes the Ag-bulk/Si contact structures of the crystalline silicon solar cells. Then, the influences of the Ag-contacts/Si-substrate on performance of the resulted solar cells are investigated. The objective of this chapter was to improve the understanding of front side contact formation by analyzing the Ag-bulk/Si contact structures resulting from different degrees of firing. The observed microscopic contact structure and the resulting solar-cell performance are combined to clarify the mechanism behind the high-temperature contact formation. Samples were fired either at a optimal temperature of ~780°C or at a temperature of over-fired for silver paste to study the effect of firing temperature. The melting characteristics of the glass frit determine the firing condition suitable for low contact resistance and high fill factors. In addition, it was found the post forming gas annealing can help overfired solar cells recover their FF. The results show that after 400°C post forming gas annealing for 25min, the over-fired cells improve their FF. On the other hand, both of the optimally-fired and the under-fired cells did not show similar

effects. The FF remains the same or even worse after post annealing. Upon overfiring, more silver dissolve in the molten glassy phase than that of optimally fired; however, some of the supersaturated silver in the glass was unable to recrystallize because of the rapid cooling process. The post annealing helps the supersaturated silver precipitate in the glass phase or on silicon surface. This helps in recovering high FF and low contact resistance. An increase in the size and number of silver crystallites at the interface and in the glass phase can improve the current transportation.

2. Overview of Ag contacts on crystalline Si solar cells

2.1 Silver paste

Currently, screen printing a silver paste followed by sintering is used for the deposition of the front contacts on almost all industrial crystalline silicon solar cells. Metallization with a silver paste is reliable and particularly fast. The silver paste have to meet several requirements: opening the dielectric antireflection layer and forming a contact with good mechanical adhesion and low contact resistance. For most crystalline silicon solar cells, SiN_x is used as an antireflection coating. The surface must be easily wetted by the paste. Figure 1 shows a typical front-electrode configuration of a commercial crystalline silicon solar cell. The electrode-pattern consists of several grid fingers that collect current from the neighboring regions and then collected into a bus bar. The bus bar has to be able to be soldered.

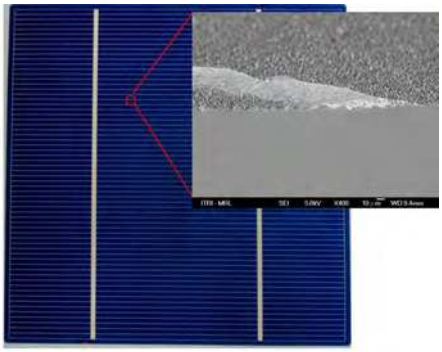

Fig. 1. A typical front-electrode configuration of a commercial crystalline silicon solar cell.

The contact performance is influenced by the paste content, the rheology and the wetting behavior.

Commercially available silver pastes generally consist of silver powders, lead-glass frit powders and an organic vehicle system. The glass frit is used to open the antireflection coating and provide the mechanical adhesion. The glass frit also promotes contact formation. The organic vehicle system primarily includes polymer binder and solvent with small molecular weight. Other additives like rheological material are also included in the paste for better printing. The paste system must have a fine line capability. This requires a well-balanced thixotropy and low flow properties during printing, drying and firing. In addition, the paste should have wide range for firing process window.

2.2 Screen printing and firing

Screen printing and the subsequent firing process are the dominant metallization techniques for the industrial production of crystalline silicon solar cells. The front contact of the cell is designed to offer minimum series resistance, while minimizing optical shadowing. The high current density of the cell can be achieved by the low shadowing loss due to the high aspect ratio of the front grid. However, a compromise between the shadowing loss and the resistive loss due to the front grid is needed. The finger-pattern with the bus bar typically covers between 6-10% of the cell surface. To achieve good performance contact, the printing parameters should be selected based on criteria directly related to the silver paste. All parameters such as the screen off-contact distance, squeegee speed and shore hardness of the squeegee rubber must be optimized and matched according to the requirements.

The industrial requirements for technical screen printing regarding excellent print performance, long screen life and higher process yields have increased significantly over recent years. The high mesh count stainless steel mesh is well suited for fine line, high volume printing. The screen should have good tension consistency and suitable flexibility required for the constant deformation associated with off-contact printing. Besides, the combinations of mesh count and thread diameter should be capable of printing the grid thickness electrode requires.

The fast firing techniques are usually applied for electrode formation. During the firing step, the contact is formed within a few seconds at peak temperature around 800°C. A typical firing profile of a commercial crystalline silicon solar cell is shown in Figure 2. The optimal firing profile should feature low series resistance and high fill factor (FF). A high series resistance of a solar cell usually degrades the output power by decreasing the fill factor. The total series resistance is the sum of the rear metal contact resistance, the emitter sheet resistance, the substrate resistance, the front contact resistance, and the grid resistance.

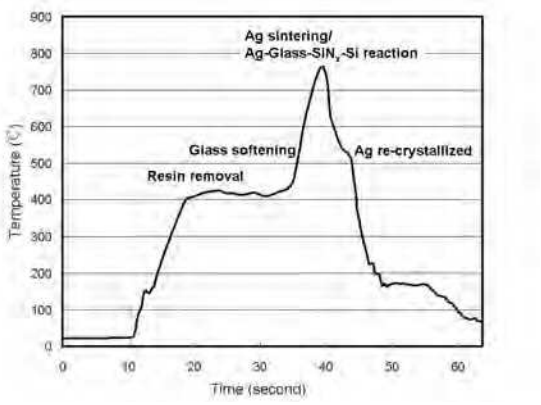

Fig. 2. A typical firing profile of a commercial crystalline silicon solar cell.

2.3 Contact mechanisms

A good front-contact of the crystalline silicon solar cell requires Ag-electrode to interact with a very shallow emitter-layer of Si. An overview of the theory of the solar cell contact resistance has been reported (Schroder & Meier, 1984). Despite the success of the screen printing and the subsequent firing process, many aspects of the physics of the front-contact

formation are not fully clear. The major reason is probably because the metal-silicon interface for screen printed fingers is non-uniform in structure and composition. The Ag particles can interact with the Si surface in a few seconds at temperatures that are considerably lower than the eutectic point.

Many mechanisms have been proposed to explain how contact formation is though to occur. The general understanding of the mechanisms agree that the glass frit play a critical role on front-contact formation. Silver and silicon are dissolved in the glass frit upon firing. When cooled, Ag particles recrystallized (Weber 2002, Schubert et al. 2004). It has been suggested that Ag crystallites serve as current pickup points and that conduction from the Ag crystallites to the bulk of the Ag grid takes place via tunneling (Ballif et al., 2003). The effect of glass frit and Ag particles on the electrical characteristics of the cell was also reported (Hoornstra et al. 2005, Hillali et al. 2005, Hillali et al. 2006). It was further suggested that lead oxide gets reduced by the silicon. The generated lead then alloys with the silver and silver contact crystallites are formed from the liquid Ag-Pb phase (Schubert et al. 2004, Schubert et al. 2006). Due to the complicate and non-uniform features of the contact interface, more evidence and further microstructure investigation is still needed. The objective of this chapter was to improve the understanding of front side contact formation by analyzing the Ag-bulk/Si contact structures resulting from different degrees of firing. The influences of the Ag-contacts/Si-substrate on performance of the resulted solar cells are also investigated.

3. Structural properties of Ag-contacts/Si-substrate

3.1 Sample preparation

This study is based on industrial single-crystalline silicon solar cells with a SiN_x antireflection coating, screen-printed silver thick-film front contacts and a screen-printed aluminum back-surface-field (BSF). The contact pattern was screen printed using commercial silver paste on top of the SiN_x antireflective-coating (ARC) and fired rapidly in a belt furnace. The exact silver paste compositions are not disclosed by the paste manufacturers. The glass frit contents are estimated from the results found in this work. The boron-doped p-type 0.5-2Ωcm, 200-230μm thick (100) CZ single-crystalline Si wafers were used for all the experiments. Si wafers were first chemically cleaned and surface texturized and then followed by $POCl_3$ diffusion to form the n^+ emitters. The resulted pyramid-shaped silicon surface is sharp and smooth, as shown in Figure 3. After phosphorus glass removal, a single layer plasma-enhanced chemical vapor deposition (PECVD) SiN_x antireflection coating was deposited on the emitters. Then, both the screen-printed Ag and the Al contacts were cofired in a lamp-heated belt IR furnace.

In this work, cells were fired either at a optimal temperature of ~780°C or at a temperature of over-fired for silver paste to study the effect of firing temperature. Some cells were further post annealed in forming gas (N_2:H_2=85:15) at 400°C for 25min. The forming gas anneal improve the fill factor (FF) for some over-fired cells.

Transmission electron microscopy (TEM) and Scanning electron microscopy (SEM) was used to study the microstructures and features at contact interface. Microstructural characterization of the contact interface was performed using a JEM-2100F transmission electron microscope (TEM) operated at 200kV. Cross-sectional TEM sample foils were prepared by mechanically thinning followed by focused-ion-beam (FIB) microsampling to electron transparency. Current-voltage (I-V) measurements were taken under a WACOM solar simulator using AM1.5 spectrum. The cells were kept at 25°C while testing.

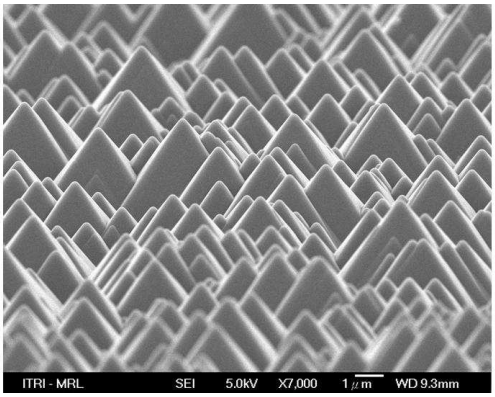

Fig. 3. SEM image of a pyramid-textured silicon surface structure

3.2 Interface microstructure

The microstructural properties of the screen-printed Ag-bulk/Si contacts were examined by TEM (Lin et al., 2008). TEM results confirmed that the glassy-phase plays an important role in contact properties. The typical Ag-bulk/Si microstructure, which includes localized large glassy-phase region, is shown in Figure 4(a). The area where Ag-bulk directly contact with Si through SEM observation is actually with a very thin glass layer (<5nm) in between as shown in Figure 4(b). This possibly can be attributed to shape-effect of Ag particles and to the existence of the glassy-phase. Ag particles do not sinter into a very compact structure and a porous Ag-bulk is formed, resulting in a complex contact structure. In this study, it was found that in optimal fired contacts, there are at least three different microstructures, illustrated in Figure 5(a)-(c) (Lin et al., 2008). The combination effects of glassy-phase and the dissolved metal atoms have a crucial influence on Ag-bulk/Si-emitter structures, and consequently, the current transport across the interface is affected.

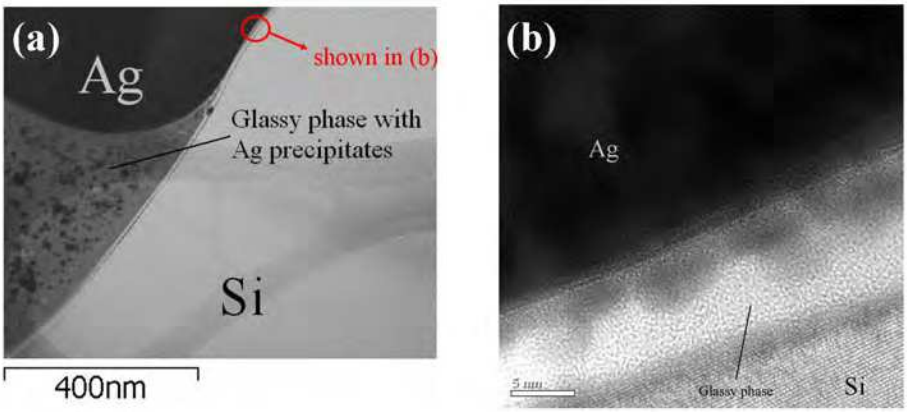

Fig. 4. (a) TEM bright field cross-sectional image of the the Ag-bulk/Si contact structure with localized large glassy-phase region. (b) HRTEM of the Ag-bulk/Si interface. There is a very thin glass layer between Si and Ag-bulk.

Figure 6 shows a high-resolution TEM (HRTEM) contrast of the Ag embryos on Si-bulk. This results in Ag-bulk/thin-glass-layer/Si contact structure which is schematic drawing in Figure 5(a). It is suggested that Ag-bulk/thin-glass-layer/Si contact structure shown in Figure 5(a) is the most decisive path for current transportation (Lin et al., 2008).

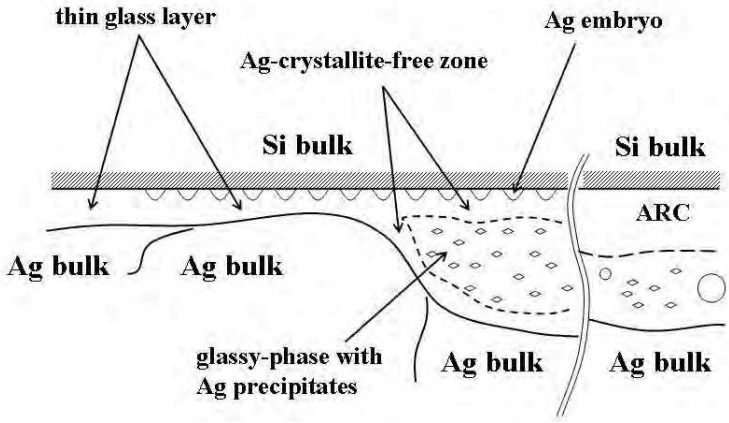

Fig. 5. Schematic drawing of the three major microstructures present in optimal fired Ag-bulk/Si contacts: (a) Ag-bulk/thin-glass-layer/Si; (b) Ag-bulk/thick-glass-layer/Si; and (c) Ag-bulk/glass-layer/ARC/Si contact structure.

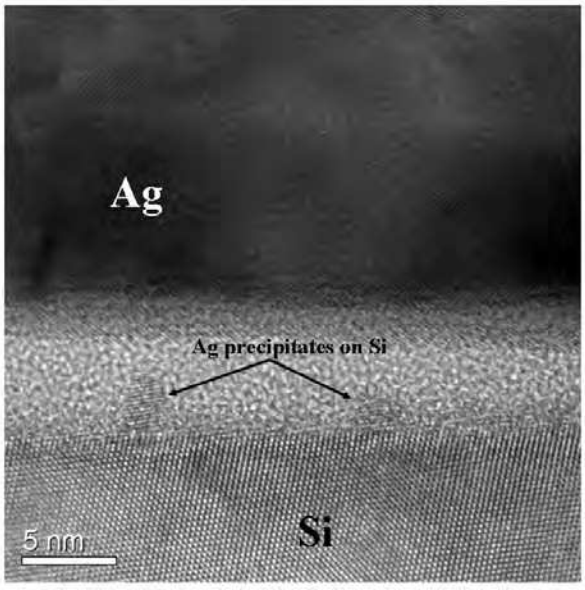

Fig. 6. HRTEM contrast of the Ag embryos on Si-bulk. This results in Ag-bulk/thin-glass-layer/Si contact structure.

The schematic Ag-bulk/thick-glass-layer/Si contact structure shown in Figure 5(b) may arise if there are large glass-frit clusters and/or large voids at the interface plane prior to high temperature treatment. Upon firing, the glass frits soften and flow all around. The flow behavior of the molten glassy-phase, to a degree, is associated with capillary attraction force caused by the tiny spacing between Ag particles, and it also depends on their wetting ability to the antireflection layer. Large and thick glassy-phase region is very likely due to the agglomeration of the molten glass frit at high temperature, and is responsible for a significant variation in glass-layer thickness.

Another interesting feature shown in Fig. 4(a) is the curve-shaped glassy-phase/Si boundary, which suggests the occurrence of mild etching of Si-bulk by the Ag-supersaturated glassy-phase. Penetration of native SiO_x and SiN_x ARC is essential for making good electrical contact with the Si emitter, thus achieving a low contact resistance. However, this must be achieved without etching all the way through the p-n junction and results in shorting the cell. It is found that a smooth curve-shaped Si surface is a distinguishable phenomenon for samples fired optimally (Lin et al., 2008). Underfired samples usually have sharp and straight interface under <110> beam direction, while rough Si surface is usually observed for overfired samples.

Even for optimally fired samples, the residual antireflection coating can be observed at some locations, especially in the valley area of the pyramid-shaped textured structure as shown in Figure 7. Amorphous antireflection layer is thus in between the glassy-phase and Si-bulk. This lead to an Ag-bulk/glass-layer/ARC/Si contact structure as illustrated in Figure 5(c). Here, ARC (~100nm thick prior to firing) includes native SiO_x layer and SiN_x ARC. To some extent, the residual SiNx under the contacts help to reduce surface recombination. Microstructures studies revealed that there is more residual ARC in underfired samples

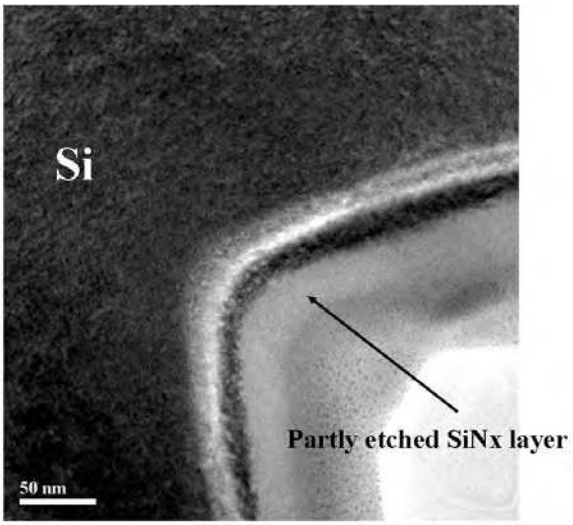

Fig. 7. TEM bright field cross-sectional image. Even for optimally fired samples, the residual antireflection coating can be observed at some locations, especially in the valley area of the pyramid-shaped textured structure. This leads to an Ag-bulk/glass-layer/ARC/Si contact structure.

than in optimally fired samples. In addition, no Ag embryo was found on Si-bulk because the residual ARC helps inhibit Ag diffusion onto Si substrate.
It is still not clear how does glassy-phase, which is a molten phase of the glass frit, etch or interact with the SiN_x ARC? It was reported that the SiN_x ARC can be opened during the firing step by a reaction between the PbO (glass) and SiN_x (Horteis et al., 2010). In the reaction, lead oxide (PbO) was reduced to lead. By tracing Pb content, this work shows that Pb precipitates usually appear in the area where SiN_x ARC can be found. That is, lead embedded in the glassy-phase with an Ag-bulk/glass-layer/ARC/Si contact structure as illustrated in Figure 5(c). The Pb concentration in glassy-phase, which originates from lead silicate glass frit, is much higher than that in ARC. Therefore, Pb can serve as a good tracer to distinguish glassy-phase-area from ARC using energy dispersive spectroscopy (EDS). Figure 8 shows Pb precipitates in the glassy phase. The inset in Figure 8 is an energy dispersive spectroscopy (EDS) mapping. This work suggests that during the firing process, the amorphous SiN_x ARC was incorporated into the already-existing glass phase. It is like two loose glassy-phase merge to each other upon firing. It is shown in this work that the SiN_x ARC in more dense structure, ex. deposited at 850°C through low-pressure CVD (LPCVD), is difficult to merge in the lead silicate glass phase.

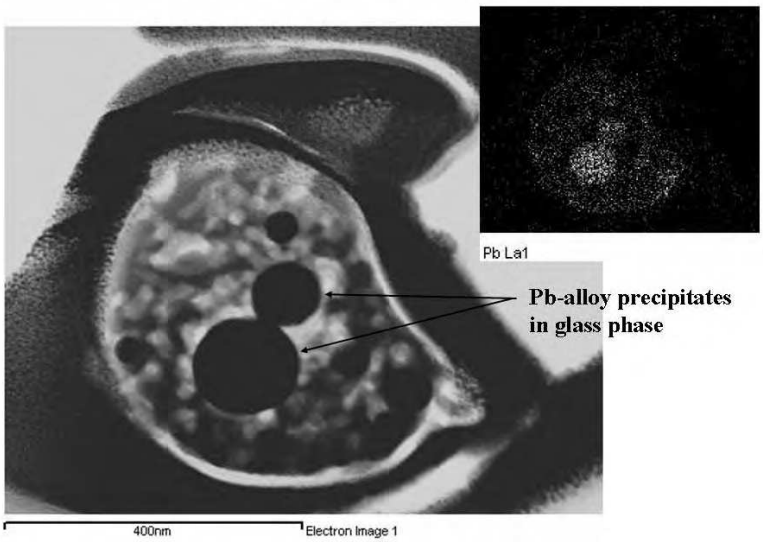

Fig. 8. TEM bright field image shows Pb precipitates in the glassy phase. The inset is the energy dispersive spectroscopy (EDS) mapping.

3.3 Crystallite-free zone in glassy phase

Commercially available Ag pastes consist of Ag powders, lead-glass frit powders and an organic vehicle system. It was found that the glass frit plays a very important role during contact formation. Upon firing, the glass frits soften and flow all around. Furthermore, the melted lead silicate glass dissolves the Ag particles. The melted glass also merges the amorphous silicon nitride layer. Upon further heating, the melted glass etches into the silicon bulk underneath and results in non-smooth silicon surface.

TEM micrographs in Figure 9(a) and (c) show the precipitates in the large solidified glassy-phase region which is enclosed with Si and Ag-bulk (Lin et al., 2008). The selected area diffraction (SAD) pattern (Figure 9(d)) reveals that only Ag precipitates exist. As shown in Figure 9(a) and its schematic drawing in Figure 9(b), the dissolved Ag atoms near Si-bulk tend to nucleate on the Si surface and lead to an Ag-crystallite-free zone in close vicinity of the Si surface. Also, an Ag-crystallite-free zone near the bulk-Ag can be found. Few or virtually no Ag microcrystallites were found in the Ag-crystallite-free zone. This indicates that the observed Ag microcrystallites are not un-melted Ag particles which were trapped or suspended in the glassy region; instead, they are precipitates from Ag supersaturation molten glassy-phase.

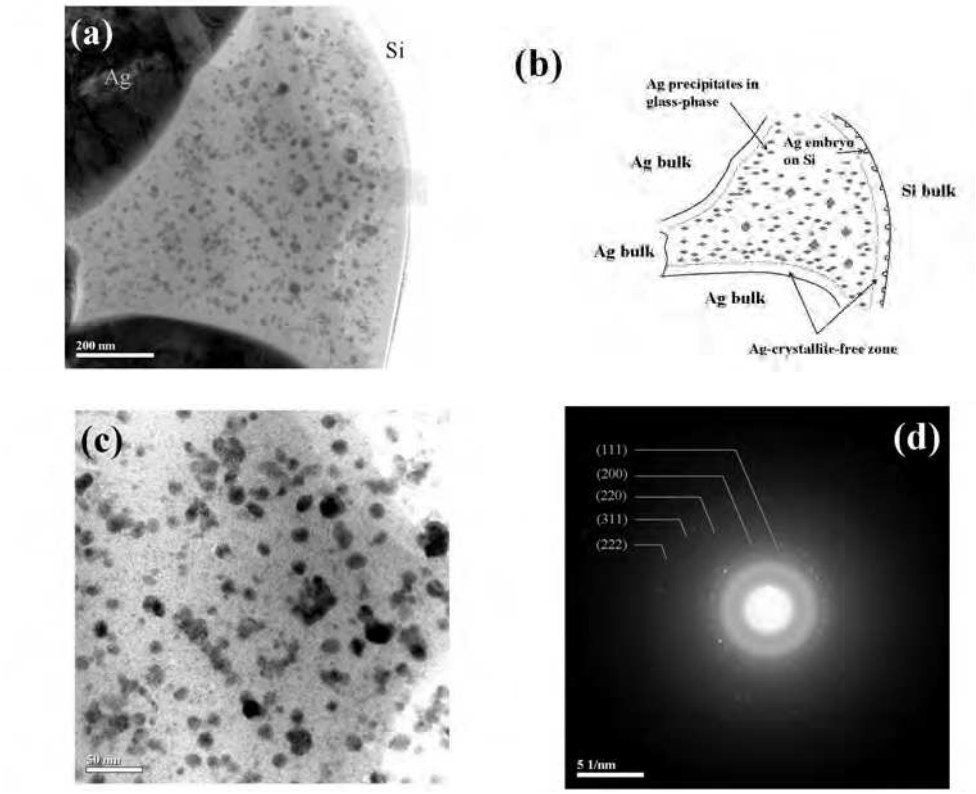

Fig. 9. (a) TEM bright field image. The large glassy-phase enclosed with Si and Ag-bulk. (b) Ag precipitates in the large solidified glassy-phase region. (c) Schematic drawing of image in (b). (d) Selected-area-diffraction pattern of the glassy-phase region shown in (b). Only Ag crystallites exist.

The occurrence of the observed Ag-crystallite-free zone can be accounted for by the diffusion-dependent nucleation mechanism (Porter and Easterling, 1981) as illustrated in Figure 10 (Lin et al., 2008). Upon heating, the dispersed lead silicate glass frits soften into molten phase, in the mean time. They further merged and surrounded the Ag particles due

to capillary attraction force. Some Ag atoms then dissolved in the molten glassy-phase. The observed Ag precipitates confirm the dissolution of Ag because a critical Ag supersaturation must be exceeded for nucleation to occur. Higher temperature increases the Ag dissolution in the glassy-phase. In the mean time, the majority un-dissolved Ag particles, which are in contact with one another, sinter or coalesce to achieve Ag-bulk via interdiffusion of Ag atoms. The molten glassy-phase can further merge (or etch) the amorphous antireflection coating and, therefore, is in direct contact with the Si-bulk. The formation of Ag-crystallite-free zone is attributed to the nucleation and growth of Ag crystallites on Si-bulk. Upon cooling, the dissolved Ag was drained from the surrounding area to Si surface and an Ag-crystallite-free zone results. The width of the Ag-crystallite-free zone is affected by the cooling rate. High cooling rate will produce narrow Ag-crystallite-free zone. This helps in tunneling-assisted carrier transportation. A narrow (width < 20nm) Ag-crystallite-free zone was observed in a large glassy-phase region for optimally fired samples.
It can be found that Ag precipitates in glassy-phase tend to coarsen into larger crystallites with smaller total interfacial area. Also, wide Ag-crystallite-free zones, which surround the large Ag precipitate, were observed. However, the combination effects of low Ag-precipitate density and wide Ag-crystallite-free zone are not favor for current transportation. It, therefore, suggests that long stay in high temperature as well as low cooling rate is of particular concern in the design of firing profile.

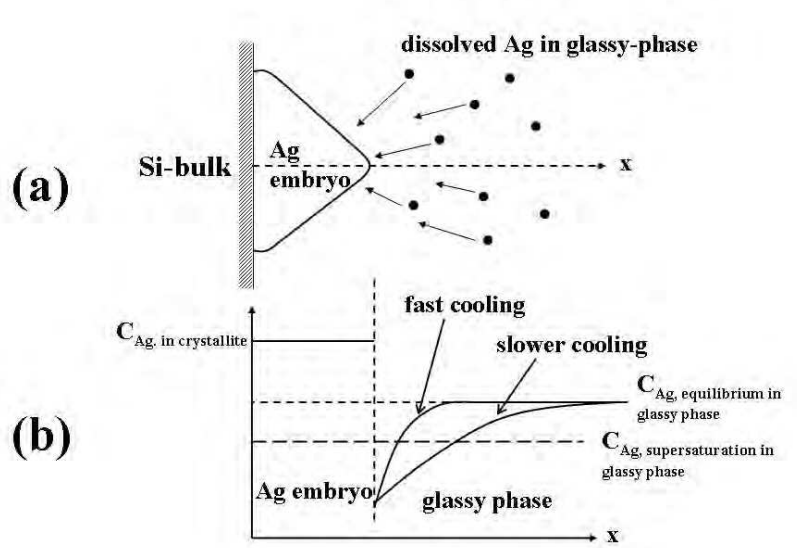

Fig. 10. (a) Schematic cross-section drawing of the Ag-embryo on Si-bulk. (b) Schematic drawing of the dissolved Ag-concentration profile near an Ag embryo.

4. Impacts of contact structure on performance of solar cell

4.1 A possible mechanism for carrier transportation

The current transport across screen-printed front-side contact of crystalline Si solar cells should be strongly affected by the contact microstructures. This study shows that the area where Ag-bulk directly contact Si, through SEM observation, is actually with a very thin glass layer in

between. In addition, high-density Ag-embryo was found on Si-bulk for samples fired optimally. In Figure 11, Ag embryos with sizes less than 5 nm in diameter nucleate epitaxially on the Si surface. The Ag-embryo density is more than $2x10^{16}cm^{-2}$, which was counted via TEM. This results in Ag-bulk/thin-glass-layer/Si contact structure. The lack of Ag-bulk/Si direct contact for optimally fired samples leads to a reasonable assumption that Ag-bulk/thin-glass-layer/Si contact structure is the most decisive path for current transporting across the interface. The glass layer between Ag-embryos and Ag-bulk for samples fired optimally is too thin (<5nm) to be an effective barrier to electron transfers, which can occur by tunneling.

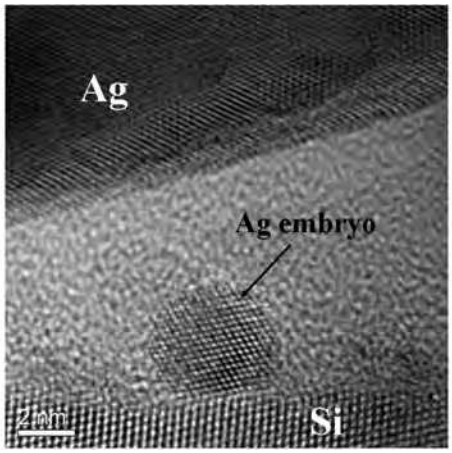

Fig. 11. Cross-sectional HRTEM of the Ag embryos on Si-bulk. This results in Ag-bulk/thin-glass-layer/Si contact structure.

The schematics of a possible conductance mechanisms across the Ag-bulk/thin-glass-layer/Si contact structure is shown in Figure 12. Current transport between Si substrate and front contact is enabled by separated silver crystallites. Since the curved regions of the tiny-pricipitate/glass-phase interface have higher field intensity due to the small radius of curvature; therefore, the breakdown voltage is less (Sze S.M., 1981). Besides the curved-interface effect mentioned above, the metal-supersaturated glassy-phase has better conductivity. The embedded metal precipitates in glassy-phase, as shown in Figure 9, can retain the charge and form the interfacial charge storage centers. In addition, the embedded Ag precipitates can be charged and discharged by quantum-mechanical tunneling of electrons. Moreover, the dissolved Ag can substantially increase the trap density at the interface, thereby allowing shorter times for the transportation. Thus, current can transport through the thick glassy-phase not only by multi-tunneling steps between Ag precipitates, but also by thermally excited electrons hopping from one isolated precipitate to the next. In the case of a current transport by multi-tunneling steps between microscopic Ag precipitates, high Ag-precipitate density in the glassy-phase could help to decrease the specific contact resistance of samples (Gzowski et al. 1982, Ballif et al. 2003).
Many of the ideas that were discussed with regard to Ag-particles/thick-glass-layer/Si microstructure can be carried over to Ag-particles/thin-glass-layer/Si (Figure 5(a)). Only the thick glassy-phase is replaced by an ultrathin glass layer, and this has important consequences for the current conduction across the interface. It was reported (Rollert et al.,

1987) that if the Ag-bulk is in direct contact with the Si and if there was no glass layer in between, the Ag would diffuse at least 5μm deep during the firing cycle and it would shunt the p-n junction. The high-density Ag-embryo on Si found in this study originates from the dissolved Ag in glassy phase, which is in direct contact with Si-bulk. This should play an important role in current transport across the interface. This could be supported by the observation of less Ag-embryo on Si was found for underfired samples, which result in poorer FF of the cell compared to those of optimally fired samples. In the case of underfired samples, the dissolution of Ag is much less; it therefore reduces the supersaturation of Ag. Thus, few Ag precipitates were detected on Si.

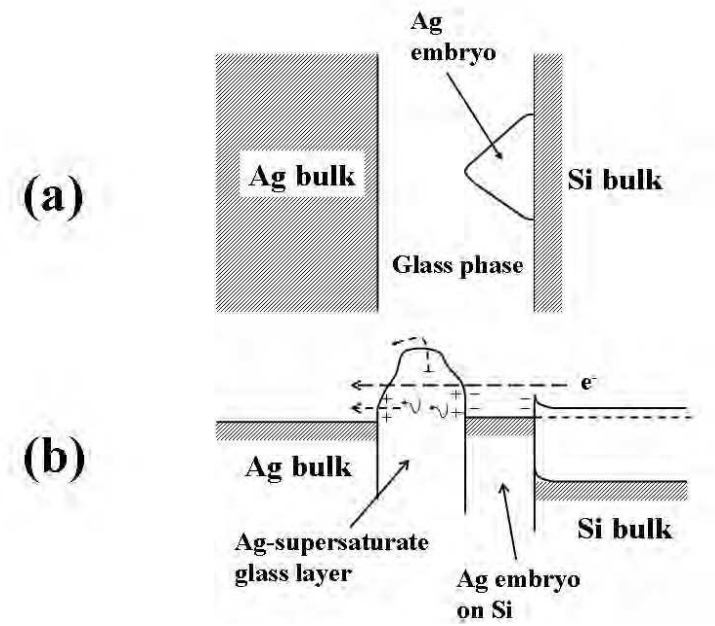

Fig. 12. (a) Schematic cross-section drawing of the Ag-embryo on Si-bulk. (b) Schematic energy-band drawing of a possible conductance mechanisms across Ag-bulk/thin-glass-layer/Si contact structure.

As shown in Figure 12, Ag-embryo on Si could serve as current pickup points and that conduction from the Ag-embryo to Ag-bulk takes place via tunneling through the ultrathin glass layer in between. An increase in the width and the number of Ag precipitates on Si may improve the probability of the encounter of thin glass regions where tunneling can take place. Also, due to tunneling-assisted carrier transport, the fraction of thin glass regions at Ag-bulk/Si interface is critical in reducing the macroscopic contact resistance. Thus, the abilities to generate high-density Ag-embryos on Si-bulk and to keep the glass layer thin are crucial in achieving good electrical contact.

It was reported (Card & Rhoderick 1971, Kumar & Dahlke 1977) that if the insulator layer is sufficiently thick, the tunneling probability through the insulator layer is negligible. Alternatively, if the insulator layer is very thin (< 5nm), little impediment is provided to carrier transport. This study confirms that the spacing between Ag-embryos and Ag-bulk can

be less than 5nm. In addition, the dissolved Ag could improve the electrical conductivity of the glass layer. It, therefore, suggest that carriers through the ultrathin glass layer are the most decisive path for current transportation. A possible mechanism for carriers passing through the thin glass layer is illustrated by considering electron tunnel, as shown in Figure 12.
The interface microstructure analysis of the screen-printed front-side contact shown in this work is based on industrial-type rapid firing-profile, which results in good contact quality. Although Ag-paste composition and characteristics can be different between manufacturers, the results and trends shown in this work have high degree similarity to other screen-printed crystalline Si solar cells using different types of Ag-paste. Further understanding of the effects of the paste constituents and firing conditions on the contact interface can lead to the development of better, more reproducible, and higher performance contacts in the future.

4.2 Effects on fill factor

The fill factor, FF, is a measure of the squareness of the I-V characteristic. The fill factor is given: $FF=(V_{max}I_{max})/(V_{oc}I_{sc})$, where V_{oc} is the open-circuit voltage and I_{sc} is the short-circuit current. V_{max} and I_{max} are voltage and current at maximum power point (P_{max}) respectively. The graphical interpretation of P_{max} is the area of the largest rectangle below the I-V curve. In practice, FF is less than one because series and parallel resistances will always result in a FF decrease. A good value for industrial silicon solar cells is ~76-78%.
It was found that the glass frit plays an important role during contact formation. During firing procedures, the glass frits firstly get fluid, wet and merge the SiNx dielectric layer. It was then etching into silicon substrate. It was known that defects and impurities tend to move to surface upon high temperature treatments to release their high thermodynamic energies. Therefore, the etching degree of silicon by the glass fluid, to some extent, affects the quality of the contacts. On cooling down, silver precipitates, which serve as a transport medium, recrystallize on silicon surface as well as in the glassy phase. This chapter shows that silver precipitates during cooling and the etching degree of silicon during firing are important for achieving good quality contacts.
On cooling down from high temperature firing, the over-saturated silver tends to precipitate. Figure 13(a) shows a SEM microstructure image of optimally fired sample. Besides precipitating in the glassy phase, high density Ag recrystallizes appear on the silicon substrate. The area where silver directly contacts to Si through SEM observation is actually with a very thin glass layer in between. The dissolved Ag atoms near Si-bulk tend to nucleate on the Si surface. Ag-embryo on Si can serve as current pickup points and that conduction from the Ag-embryo to Ag-bulk takes place via tunneling through the ultrathin glass layer in between. Thus, the abilities to generate high density Ag embryos on Si-bulk and to keep the glass layer thin are crucial in achieving good electrical contact. The observed Ag precipitates confirms the dissolution of Ag because a critical Ag supersaturation must be exceeded for nucleation to occur. In the case of underfiring, the less dissolved Ag reducing the supersaturation, and therefore, fewer Ag precipitates grow on Si during cooling as shown in Figure 13(b).
Penetration of native SiO_x and SiN_x antireflective coating is essential for making good electrical contact to the Si emitter, thus achieving a low contact resistance. However, this must be achieved without etching all the way through the p-n junction and results in shorting the cell. It is found that a smooth curve-shaped Si surface is a distinguishable phenomenon for samples fired optimally. Underfired samples usually have sharp and straight interface, while rough Si surface is usually observed for overfired samples. As shown in Figure 14(a) and (b), overfiring results in rough Si surface. Rough Si surface

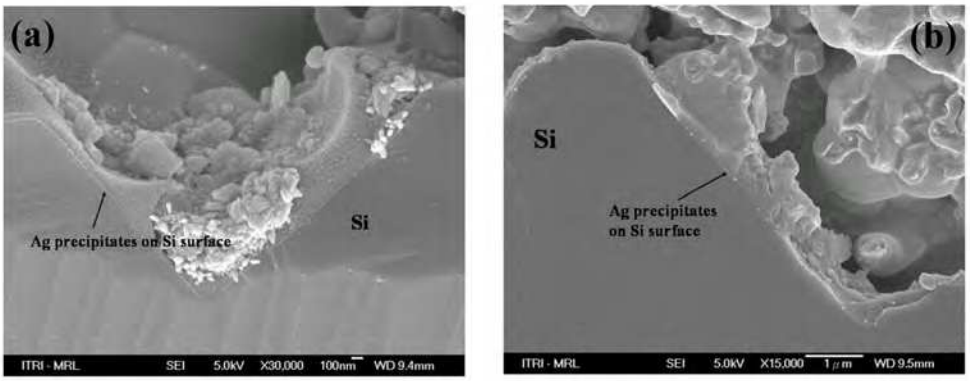

Fig. 13. (a) SEM cross-sectional image of the optimally fired sample. Besides precipitating in the glassy phase, high density Ag recrystallizes on the <111> planes of the pyramid Si. (b) SEM cross-sectional image of the underfired sample. Fewer Ag precipitates grow on Si.

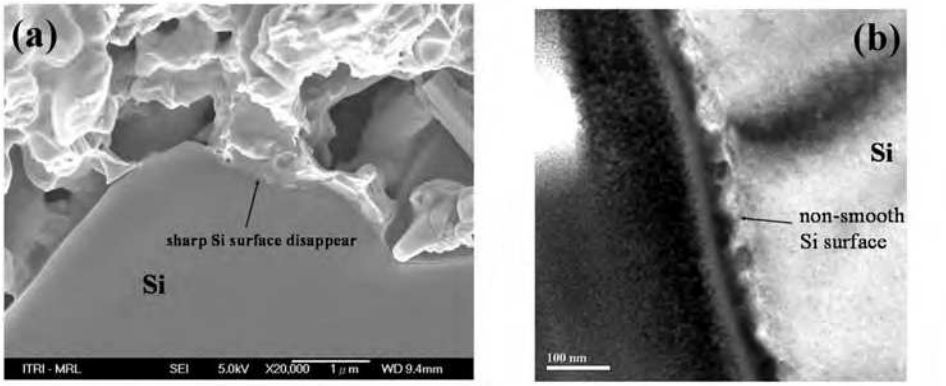

Fig. 14. (a) SEM cross-sectional image of the overfired sample. More bulk Si, especially in the area near the tip of the pyramid, was etched during firing. (b) TEM bright field cross-sectional image of the overfired sample.

increase the possibility of undesired surface recombination. Furthermore, as shown in Figure 14(a), more bulk Si, especially in the area near the tip of the pyramid, was etched during firing. The overetching of Si may result in locally shunt of the cell.

In general, the relation between the current density through the contact and the potential across it is non-linear for metal-semiconductor contacts (Schroder and Meier, 1984). The metal-silicon interface for screen printed fingers is known to be non-uniform in structure and composition. It is found the melting characteristics of the glass frit and its ability to dissolved Ag have significant influence on contact resistance and fill factors (FF). Glass frit advances sintering of the Ag particles, wets and merges the antireflection coating. Moreover, glass frit forms a glass layer between Si and Ag-bulk, and can further react with Si-bulk and forms pin-holes on the Si surface upon high temperature firing. Typical firing temperatures of a commercial solar cell were between 750C and 800C, where the optimum balance between the Ag-crystallite density and the distribution of the glass layer should be found.

For optimum solar cell efficiency, the current-voltage curve must be as rectangular as possible. The new paste design should increase the fill factor of the solar cell without hurting the short-circuit current density. The current-voltage (I-V) characteristic of an ideal silicon solar cell is plotted in Figure 15 denoted as curve-1. In Figure 15, Curve-2 shows the effect of shunt resistance on the current-voltage characteristic of a solar cell (series resistance R_s=0). The shunt resistance, R_{sh}, has little effect on the short-circuit current, but reduces the open-circuit voltage. Curce-3 shows the effect of series resistance on the current-voltage characteristic of a solar cell ($R_{sh}\rightarrow\infty$). Conversely, the series resistance, R_s, has no effect on the open-circuit current, but reduces the short-circuit current. Sources of series resistance include the metal contacts. The extreme current-voltage characteristic, ex. Curve-2 or Curve-3 shown in Figure 15, is not difficult to explain. However, the original sources for I-V curve denoted as Curve-4 in Figure 15 remain unclear. It is not unusually to have I-V feature similar to that of Curve-4. The difference between the curve-1 and curve-4 (the rounded corner of the I-V curve) is probably due to the non-uniform contact resistance of the front contact. Although it is known that the curve can be rounded by series resistance, in practice curve shapes are often found that cannot be explained by the single series resistance.

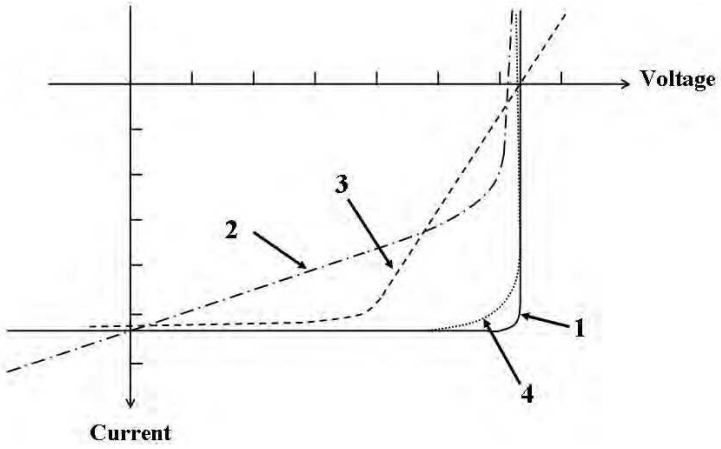

Fig. 15. Current-voltage (I-V) characteristic of a silicon solar cell. The I-V curve for an ideal cell is denoted as curve-1.

The front-contact interface for screen printed fingers is non-uniform in structure and composition. The complicate interface-structure influences the series resistance and the fill factor of the cell. From the view of contact-formation mechanism described in this chapter, the melting characteristics of the glass frit determine whether the paste together with the firing condition is suitable for low contact resistance and high fill factors.

It was found the post forming gas annealing can help overfired solar cells recover their F.F. The results show that after 400°C post forming gas annealing for 25min, the overfired cells improve their FF. On the other hand, both of the optimally-fired and the under-fired cells did not show similar effects. The FF remains the same or even worse after conducting post-annealing.

The mechanism of FF recovers for overfired cells after post forming-gas annealing was further investigated. It was found that the supersaturated silver in the glassy-phase plays a very important role for FF recover. More Ag can dissolve in the molten glassy phase for overfired samples than that of optimally fired counterparts. Either higher temperature or

longer heating time increases the Ag dissolution in the glassy-phase. Some of the supersaturated silver in the glass for overfired cells was unable to recrystallize because of the rapid cooling process. The post-annealing helps the supersaturated silver further precipitate in the glassy-phase or move to already exist Ag crystallites. The number of small precipitates is increased and the conductivity of the insulating glass is improved. Post-annealing the overfired cells thus results in recovering high FF and low contact resistance. An increase in the size and number of silver crystallites at the interface and in the glass phase can improve the current transportation.

Post-annealing of overfired cells helps the supersaturated Ag precipitate. It also coalesce the pre-formed Ag crystallites. More Ag embryos were generated and grew to larger size, which decreased the contact resistance, and enhanced the F.F. As shown in Table 1, the forming-gas anneal reduces the contact resistance, and thus, it improves the FF for the overfired cells. In Table 1, the post-annealing increases the FF by 1.5~9%. However, it should be mentioned that the cells cannot be overfired too much. It must be avoided to etch all the way through the p-n junction, which results in shorting the cell. The overetching of Si underneath may result in locally shunt of the cell. Besides, overfiring results in rough Si surface. Rough Si surface increase the possibility of undesired surface recombination.

Sample #	ΔJsc/Jsc (%)	ΔVoc/Voc (%)	ΔFF/FF (%)	ΔEff/Eff (%)
1	-0.68	-0.25	2.66	1.71
2	-0.30	-0.27	1.75	1.16
3	-0.36	-0.05	4.68	4.25
4	-1.92	-0.61	3.19	0.58
5	-0.01	-0.68	9.13	8.38

Table 1. The forming gas anneal improves the FF for the overfired cells.

The mechanism for FF enhancement of the overfired cells after post-annealing is related to the supersaturated Ag. Figure 16(a) shows a HRTEM image of the silicon/electrode

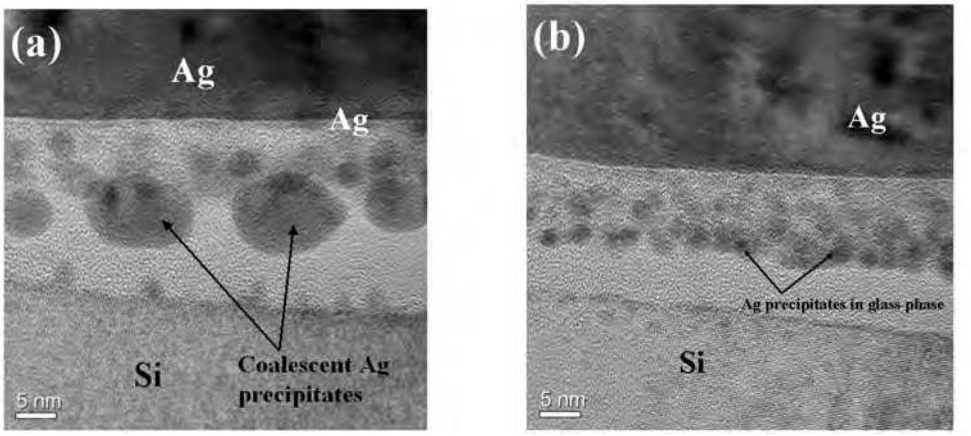

Fig. 16. (a) HR TEM contrast of more and large Ag crystallites in the glassy phase. (b) HR TEM contrast of contact interface. Ag precipitates are closer to Ag-bulk.

interface structure. It can be found that the Ag crystals in the glassy phase grow to larger size either by electron beam annealing or by heat treatments, indicating a better current transportation. The Ag area coverage at the Si-Ag interface is increased. More and larger Ag crystallites in the glassy phase increase the contact area fraction, which improves the probability of tunneling from Ag crystallites to the Ag bulk. The better conductance contributes to lower contact resistance and a higher FF. Also shown in Figure 16(b), more Ag embryos were generated and result in a locally decreased contact resistance. The rounded-corner feature of the I-V curve, as shown as Curve-4 in Figure 15, can be improved. The rounded-corner feature of the I-V curve is caused by combination effects of resistance and recombination. Control the process better and decrease the carriers' jumping-path can improve the fill factor of the cell.

5. Conclusion

Despite the success of the screen printing and the subsequent firing process, many aspects of the physics of the front-contact formation are not fully clear. The major reason is probably because the contact-interface for screen printed fingers is non-uniform in structure and composition. The contact microstructures have a high impact on current-transport across the contact-interface.

This chapter first presents the Ag-bulk/Si contact structures of the crystalline silicon solar cells. Then, the influences of the Ag-contacts/Si-substrate on performance of the resulted cells are investigated. The objective of this work was to improve the understanding of front-side contact formation by analyzing the individual contact types and their role in the Ag-bulk/Si contact. Microstructure analyzing confirmed that the glassy-phase plays an important role in contact properties. The location where Ag-bulk directly contact Si-substrate, through SEM observation, is actually a very thin glass layer in between. High density Ag-embryos on Si-bulk were found for samples fired optimally. It is suggested that Ag-bulk/thin-glass-layer/Si contact is the most decisive path for current transportation. Possible conductance mechanisms of electrons across the contact interface are also discussed.

Ag-embryo on Si could serve as current pickup points and that conduction from the Ag-embryo to Ag-bulk takes place via tunneling through the ultrathin glass layer in between. Thus, the abilities to generate high density Ag embryos on Si-bulk and to keep the glass layer thin are crucial in achieving good electrical contact.

This chapter also reports that after 400°C post forming-gas annealing for 25min, the overfired cells improve their FF. The mechanism for FF enhancement of the overfired cells after post-annealing is related to the supersaturated silver in glassy-phase. The post-annealing helps the supersaturated silver further precipitate in the glassy-phase or move to already exist Ag crystallites. More and larger Ag crystallites in the glassy phase increase the contact-area fraction, which improves the probability of tunneling from silver crystallites to the silver bulk.

The interface microstructure analysis of the screen-printed front-side contact shown in this work is based on industrial-type rapid firing-profile. Although Ag-paste composition and characteristics can be different per manufacturer, the results and trends shown in this work have high degree similarity to other screen-printed cell using different type Ag-paste. Further understanding the effects of the paste constituents and firing conditions on the contact-interface can lead to develop a better, more reproducible, and higher performance screen-printed electrode.

6. Acknowledgements

It is gratefully acknowledged that this work has been supported by Bureau of Energy, Ministry of Economics Affairs, Taiwan. The authors would also like to thank Shu-Chi Hsu and Chih-Jen Lin for their TEM operation.

7. References

Ballif C., D. M. Huljić, G. Willeke, and A. Hessler-Wysser (2003). Silver thick-film contacts on highly doped n-type silicon emitters: structural and electronic properties of the interface, *Applied Physics Letters*, Vol. 82, pp. 1878-1880. ISSN 0003-6951.

Card H.C. and E. H. Rhoderick (1971). Studies of tunnel MOS diodes I. Interface effects in silicon Schottky diodes, *Journal of Physics D: Applied Physics*, Vol. 4, pp. 1589.

Gzowski O., L. Murawski, and K. Trzebiatowski (1982). The surface conductivity of lead glasses, *Journal of Physics D: Applied Physics, Vol*. 15, pp. 1097-1101.

Hilali M.M., K. Nakayahiki, C. Khadilkar, R. C. Reedy, A. Rohatgi, A. Shaikh, S. Kim, and S. Sridharan (2006). Effect of Ag particle size in thick-film Ag paste on the electrical and physical properties of screen printed contacts and silicon solar cells, *Journal of The Electrochemical Society*, Vol. 153, pp. A5-A11. ISSN 0013-4651.

Hilali M.M., M. M. Al-Jassim, B. To, H. Moutinho, A. Rohatgi, and S. Asher (2005). *Journal of The Electrochemical Society,* Vol. 152, pp. G742-G749. ISSN 0013-4651.

Hoornstra J., G. Schubert, K. Broek, F. Granek, C. LePrince (2005). Lead free metallization paste for crystalline silicon solar cells: from model to results, *31st IEEE PVSC conference*, Orlando, Florida.

Horteis M, T. Gutberlet, A. Reller, and S.W. Glunz (2010). High-temperature contact formation on n-type silicon: basic reactions and contact model for seed-layer contacts, *Advanced Functional Mateials*, Vol. 20, pp. 476-484.

Kumar V. and W. E. Dahlke (1977), Solid State Electron., Vol. 20, pp. 143.

Lin C.-H., S.-Y. Tsai, S.-P. Hsu, and M.-H. Hsieh (2008). Investigation of Ag-bulk/glassy-phase/Si heterostructures of printed Ag contacts on crystalline Si solar cells, *Solar Energy Materials & Solar Cells*, Vol. 92, pp. 1011-1015.

Porter D.A. and K.E. Easterling (1981), *Phase Transformations in Metals and Alloys*, Chapman & Hall, New York.

Rollert F., N. A. Stolwijk, and H. Mehrer (1987), Solubility, diffusion and thermodynamic properties of silver in silicon, *Journal of Physics D: Applied Physics*, Vol. 20, pp. 1148-1155.

Schroder D.K. & Meier D.L. (1984). Solar cell contact resistance – a review, *IEEE Transactions on Electron Devices*, Vol. 31, pp. 637-647. ISSN 0018-9383.

Schubert G., F. Huster, P. Fath (2004), Current Transport Mechanism in printed Ag Thick Film Contacts to an n-type Emitter of a Crystalline Silicon Solar Cell, *Proceedings of 19th European Photovoltaic Solar Energy Conference*, Paris, France, pp. 813-817.

Schubert G., F. Huster, and P. Fath (2006). Physical understanding of printed thick-film front contacts of crystalline Si solar cells—Review of existing models and recent developments, *Solar Energy Materials & Solar Cells*, Vol. 90, pp. 3399-3406.

Sze S.M.(1981). *Physics of Semiconductor Devices*, 2nd Edition, John Wiley & Sons, New York, ISBN 10-0471-0566-18.

Weber L. (2002), Equilibrium solid solubility of silicon in silver, *Metallurgical and Materials Transactions A*, Vol. 33, pp. 1145-1150.

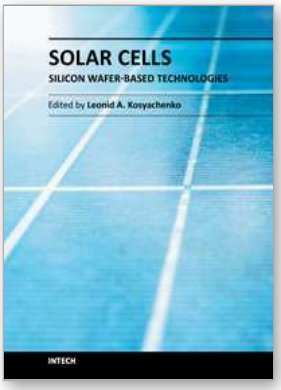

Solar Cells - Silicon Wafer-Based Technologies

Edited by Prof. Leonid A. Kosyachenko

ISBN 978-953-307-747-5
Hard cover, 364 pages
Publisher InTech
Published online 02, November, 2011
Published in print edition November, 2011

The third book of four-volume edition of 'Solar Cells' is devoted to solar cells based on silicon wafers, i.e., the main material used in today's photovoltaics. The volume includes the chapters that present new results of research aimed to improve efficiency, to reduce consumption of materials and to lower cost of wafer-based silicon solar cells as well as new methods of research and testing of the devices. Light trapping design in c-Si and mc-Si solar cells, solar-energy conversion as a function of the geometric-concentration factor, design criteria for spacecraft solar arrays are considered in several chapters. A system for the micrometric characterization of solar cells, for identifying the electrical parameters of PV solar generators, a new model for extracting the physical parameters of solar cells, LBIC method for characterization of solar cells, non-idealities in the I-V characteristic of the PV generators are discussed in other chapters of the volume.

How to reference

In order to correctly reference this scholarly work, feel free to copy and paste the following:

Ching-Hsi Lin, Shih-Peng Hsu and Wei-Chih Hsu (2011). Silicon Solar Cells: Structural Properties of Ag-Contacts/Si-Substrate, Solar Cells - Silicon Wafer-Based Technologies, Prof. Leonid A. Kosyachenko (Ed.), ISBN: 978-953-307-747-5, InTech, Available from: http://www.intechopen.com/books/solar-cells-silicon-wafer-based-technologies/silicon-solar-cells-structural-properties-of-ag-contacts-si-substrate

INTECH
open science | open minds

InTech Europe
University Campus STeP Ri
Slavka Krautzeka 83/A
51000 Rijeka, Croatia
Phone: +385 (51) 770 447
Fax: +385 (51) 686 166
www.intechopen.com

InTech China
Unit 405, Office Block, Hotel Equatorial Shanghai
No.65, Yan An Road (West), Shanghai, 200040, China
中国上海市延安西路65号上海国际贵都大饭店办公楼405单元
Phone: +86-21-62489820
Fax: +86-21-62489821

© 2011 The Author(s). Licensee IntechOpen. This is an open access article distributed under the terms of the Creative Commons Attribution 3.0 License, which permits unrestricted use, distribution, and reproduction in any medium, provided the original work is properly cited.